ACS APPLIED MATERIALS & INTERFACES

Research Article

www.acsami.org

# Nanoporous GaN–Ag Composite Materials Prepared by Metal-Assisted Electroless Etching for Direct Laser Desorption-Ionization Mass Spectrometry

Bei Nie,[†] Barrett K. Duan,[†] and Paul W. Bohn*[,†,‡]

[†]Department of Chemistry and Biochemistry, University of Notre Dame, Notre Dame, Indiana 46556, United States

[‡]Department of Chemical and Biomolecular Engineering, University of Notre Dame, Notre Dame, Indiana 46556, United States

Supporting Information

**ABSTRACT:** Three-dimensional nanoporous gallium nitride-(PGaN) produced by metal-assisted electroless etching is chemically embedded with silver nanoparticles via electroless deposition, forming a metallized semiconductor membrane with large surface area and nanoscale metal features. A new application utilizing the unique chemical and morphological features of these composite nanostructures is described here, laser induced desorption-ionization(LDI) of biomolecules(e.g., cholesterol and nucleotides) for direct mass analysis, without use of additional organic matrix. Although PGaN itself is a poor matrix for direct LDI mass spectrometry, the combination of Ag and PGaN greatly improves ion signals relative to PGaN or Ag nanostructure surfaces alone. This behavior is attributed to the combination of strong UV absorption, enhanced surface area, and favorable thermal properties of PGaN. Importantly, Ag-PGaN is shown to facilitate the formation of Ag adduct ions in some cases, for example adenine, where adducts are not observed from either porous anodic aluminum membranes or surfaces presenting Ag nanoparticles in isolation. Nanopore-embedded Ag nanostructures serve a dual role: as cationization agents and to assist thermal desorption under UV laser irradiation. The results reported here suggest that the combination of Ag nanostructures embedded in PGaN has the capacity for high quality matrix-free LDI mass analysis.

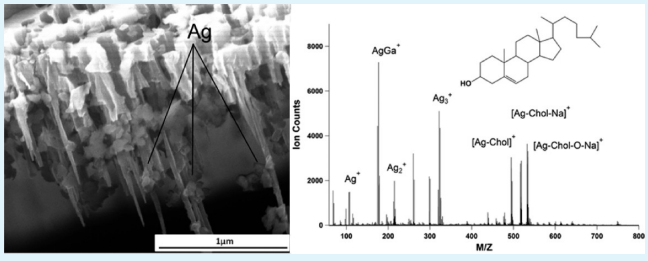


**KEYWORDS:** *porous semiconductors, gallium nitride, laser desorption–ionization, nanoparticles, mass spectrometry*

## INTRODUCTION

Nanoporous semiconductors, especially porous Si, have garnered significant attention for applications in optoelectronics,[1−4] as compliant substrates in epitaxial growth of semiconductors,[5,6] as a sacrificial layer in micromachining applications,[7] as substrates for heterogeneous catalysis,[8] and in drug delivery.[9] Interestingly, they have also attracted attention for applications in chemical sensing,[10−14] and, when decorated with metals, as substrates for surface-enhanced Raman scattering.[15−18] In addition, some porous semiconductors have proven effective as substrates for mass spectrometry.[19−21] All of these applications can ultimately be traced back to the unusual combination of structural, optical, electronic, and chemical properties possessed by nanoporous semiconductors.

In particular, porous gallium nitride(PGaN), is a compelling alternative to conventional silicon based materials, due to its wide band gap(3.4 eV) and robust physical properties. Thus, it has been utilized for a wide range of applications in electronics[22] and optics.[23,24] For example, it serves as an efficient photoanode for solar-powered water splitting, converting alternative energy sources to fuel, without emitting $CO_2$.[25] Furthermore, the preparation of composite nanostructures, either through metallization or chemical functionalization, can significantly enhance these nanoporous structures. As an example, noble metal nanostructures have been coated within PGaN nanocavities, yielding plasmonic networks that support surface-enhanced Raman detection by coupling to strong localized surface plasmon resonance(LSPR) modes of the metal nanoparticles.[18,26] Following the same protocols, catalytic metals, for example, Pt or Pd, can be deposited in contact with PGaN for catalysis and chemical sensing.[11,27,28] Similar approaches have been used to produce Schottky diodes on PGaN resulting in high sensitivity photon detectors.[29,30]

Despite these successes, direct chemical analysis from porous substrates is still largely undeveloped. Raman scattering has been utilized on metallized PGaN films for study of surface-bound analytes, however, Raman scattering typically provides information about molecular functional groups, and is not usually capable of unequivocal molecular identification. Laser desorption/ionization mass spectrometry(LDI-MS), on the other hand, is able to analyze organic compounds and biomolecules with sensitivity and chemical-fidelity.[31] More importantly, because it is resistant to interference from small matrix molecules, LDI produces high quality spectra and

Received: April 1, 2013
Accepted: June 13, 2013
Published: June 13, 2013

  

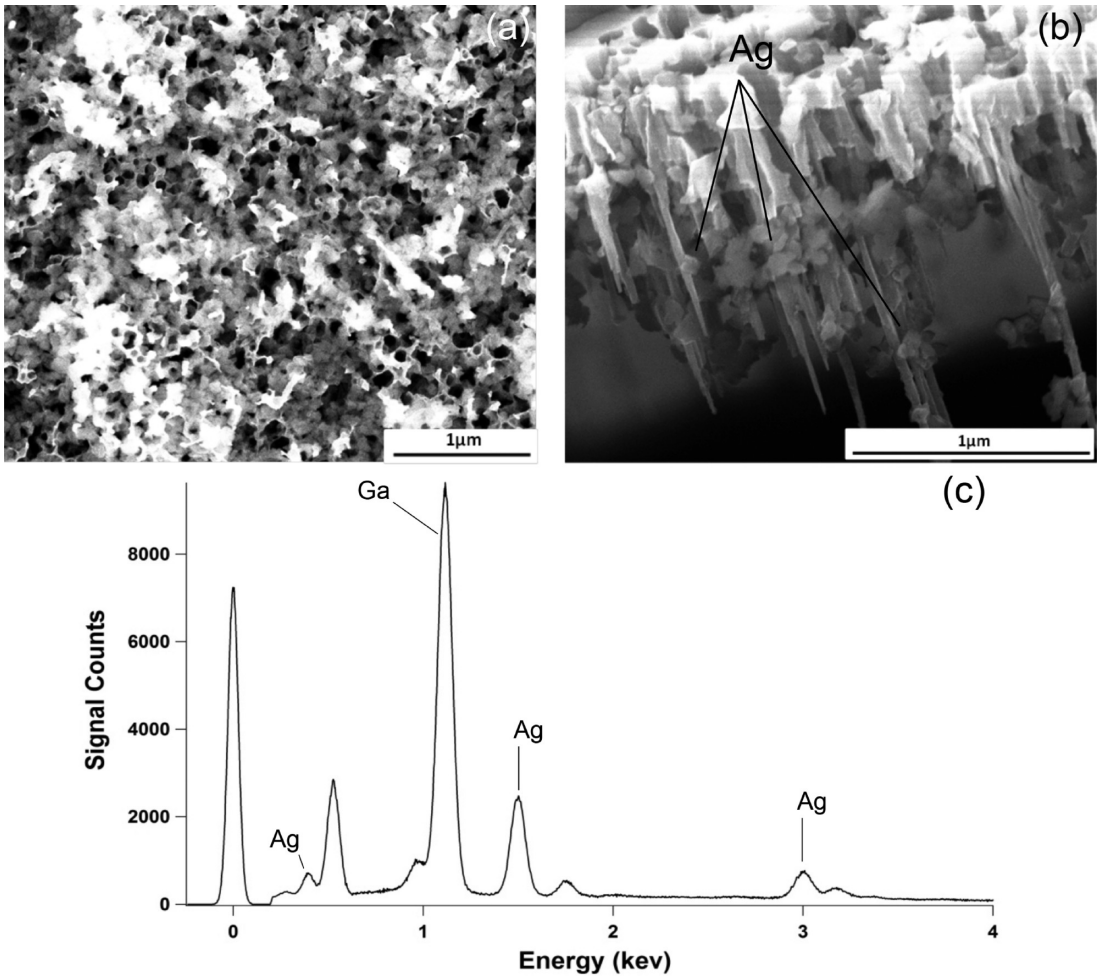


**Figure 1.** (a) Plan-view SEM micrograph of Ag-coated nanoporous GaN film(12 $\mu$m-thick, $n \approx 2 \times 10^{18}$ cm$^{-3}$) grown on sapphire. The nanoporous structure is sculpted by Pt-assisted MacEtch, and Ag nanostructures are subsequently deposited using electroless metal plating.(b) Cross-section image of surface-bounded Ag nanostructures on the interior of PGaN, showing the deposition of Ag nanoparticles and clusters deep within the GaN nanopores.(c) Energy-dispersive X-ray spectrum of Ag-PGaN composite film.

accurate mass analysis in relatively low mass regions(<500 Da). Thus, a number of materials have been used to obtain LDI-MS of small molecules, including titania sol−gels,[32] graphite,[33,34] graphene,[35] coinage metal nanoparticles, and a variety of nanostructures.[36,37] High density, moderate bandgap nanostructures are attractive supports for LDI, because they can absorb UV photons, rapidly transfer thermal energy, and thereby initiate analyte desorption and subsequent ionization.[38,39] Thus, PGaN would appear to be a useful LDI substrate, with its large surface area, high aspect ratio pore structure, bandgap well matched to lasers typically used in MALDI, high heat capacity, and thermal conductivity.[40] Unfortunately, compared to LDI on porous silicon, previous attempts to achieve LDI on PGaN have been disappointing.[20]

One hypothesis ties the lackluster LDI performance of PGaN to the lack of intrinsic cationization agents, such as protons or alkali metal cations, on GaN surfaces, providing a rationale for metallizing PGaN with Ag by electroless deposition to combine the strong UV-absorbance of GaN with a $Ag^+$ cationization agent. This report describes a protocol for producing a Ag-PGaN composite material on which LDI mass spectrometry may be performed directly. PGaN films are first fabricated by metal-assisted electroless chemical etching[41−44] and are coupled with two different Ag-coating methods, electroless Ag deposition and argon/oxygen plasma sputtering, to form Ag-embedded PGaN nanostructures. Although bare PGaN is unable to facilitate LDI, adding Ag nanostructures produces strong LDI signals for a variety of small molecules. Here we explore the use of Ag-PGaN composite nanostructures as LDI substrates with an emphasis on the materials characteristics that affect signal strength.

## EXPERIMENTAL SECTION

**Materials.** All chemical reagents were ACS reagent grade and used as received. The crystalline GaN films were 12 $\mu$m thick, *n*-type, $[Si_{Ga}] = (1-3) \times 10^{18}$ cm$^{-3}$, and were purchased from TDI, Oxford Instruments, Inc.(Silver Spring, MD). All chemicals, including solid $AgNO_3$, $SnCl_2$, $NH_4OH$, trifluoroacetic acid, $NaHCO_3$, $Na_2SO_3$, and formaldehyde were ordered from Sigma-Aldrich and used as received. Cholesterol was obtained from Avanti Polar Lipids and stored at −20 °C until ready for use. Immediately after opening the glass shipping vial, the solid white lipids were dissolved in methanol and diluted to 1 mg/mL, creating a stock solution for future use. Deionized (DI) water($\rho$ = 18 MΩ cm) was produced using a Milli-Q Gradient water purification system(Millipore, Bedford, MA).

**Porous GaN Fabrication.** Nanoporous GaN structures were created by metal-assisted chemical etching.[18,42,45] The GaN substrates were cleaned in concentrated aqua regia for 15 min, rinsed in DI water and $CH_3OH$, and dried with $N_2$. Pt islands(8 nm thickness) were sputter-coated with a Desk IV sputter coater(Denton Vacuum),


dx.doi.org/10.1021/am401132s | ACS Appl. Mater. Interfaces 2013, 5, 6208−6215

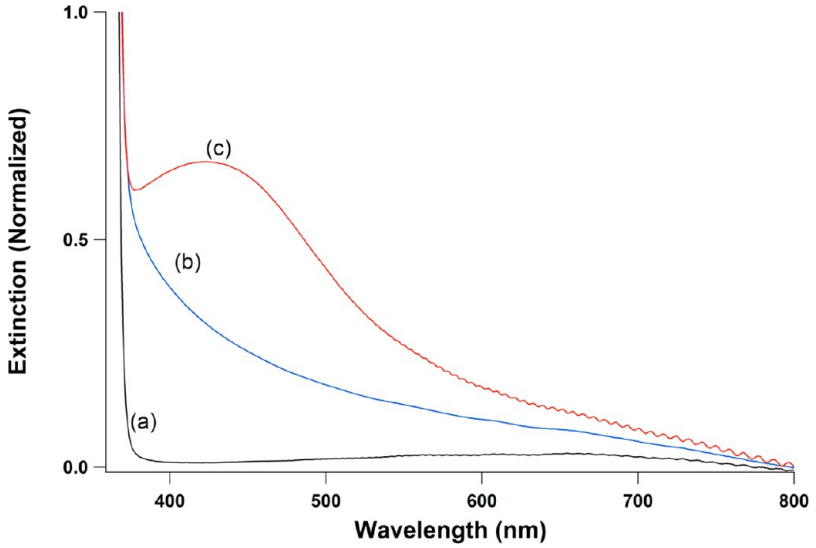


**Figure 2.** Representative UV−visible extinction spectra of various chemically treated GaN thin films. (a) Unetched crystalline GaN, (b) PGaN film, and (c) Ag-decorated PGaN.

forming a parallel array of 1 mm diameter circles. The GaN substrate was then etched in a solution of $CH_3OH$, HF(Transene Co., 49% semiconductor grade), and $H_2O_2$ with a volume ratio of 1:2:2 under a 100 W Hg lamp(Oriel Instruments model 6182, Oriel Instruments 68806 power supply) for 60 min.(*Caution: Aqua regia is only effective immediately following preparation. It should be neutralized promptly after use and should not be stored in a closed container. Use only plastic containers and tools when handling HF. In addition to standard laboratory personal protective equipment, an acid resistant apron, face shield, and heavy nitrile or neoprene gloves must be worn when handling HF*). After etching, the samples were rinsed in several successive cycles of DI water and methanol, then sonicated in methanol for 10 min to remove the ridge structures created during etching, resulting in uniform anisotropic porous structures.

**Electroless Deposition of Silver Nanostructures.** Ag was deposited inside the nanopores of PGaN and anodic aluminum oxide(AAO) films using a procedure modified from that used for Pt electroless deposition in PGaN.[11] Substrates were first sensitized in a fresh solution composed of 22 mM $SnCl_2$ and 67 mM trifluoroacetic acid in 1:1 (v/v) methanol:water for ∼45 min. Following sensitization, the films were thoroughly rinsed with methanol and subsequently, with water. After air drying, the films were activated in 35 mM $Ag(NH_3)_2^+$, prepared by dissolving $AgNO_3$ in water to produce a 35 mM solution, and then titrating with 37% aqueous $NH_3$ until the brown silver oxide precipitate disappeared. Exposure to this solution resulted in deposition of Ag, after which the product was again rinsed with ample methanol and water. In the final step, the activated films were exposed to a Ag plating solution, in which the concentration of formaldehyde (reductant) was adjusted from 0.3 mM to 10 mM in order to control the deposition speed. The plating was carried out at 4 °C for times ranging from 10 s to a few hours, depending on the formaldehyde concentration and desired thickness of the Ag layer.

**LDI Mass Spectrometry.** All MS experiments were performed on a Bruker-Dalton Autoflex III MALDI TOF-TOF instrument equipped with a frequency-tripled Nd:YAG laser producing 355 nm pulses at 100 Hz. The mass spectrometer was set to positive reflection mode with 20 kV accelerating voltage. All spectra were acquired and integrated over 200 shots. For data comparison, the laser fluence was maintained at ∼30 mJ $cm^{-2}$. For LDI from Ag-PGaN, low UV fluence was found to produce optimal analyte ionization while minimizing background from metal substrate. For the small molecules employed here, optimized signal-to-background response was obtained in the range 20−30 mJ $cm^{-2}$. Data were recorded by resident Autoflex software and exported into Igor Pro 6.1(Wavemetrics) for further analysis.

**SEM Characterization.** SEM micrographs of the Ag-PGaN structures were obtained on an FEI Magellan nanoscope equipped with both a field-free line detector(for large area imaging) and a high resolution backscatter detector(for <50 $\mu$m diameter regions). Instrument parameters were set to: electron beam voltage, 5 kV; working distance, 4.2 mm; working current, 29 pA. All samples were cleaned by low-power $O_2$ plasma to remove carbon-based contamination prior to SEM imaging.

## RESULTS AND DISCUSSION

**General Considerations.** Despite the positive morphological features, large heat capacity, and thermal conductivity of PGaN, previous attempts to obtain mass spectra from undecorated GaN and PGaN were largely unsuccessful, even for small metabolites and short-chain nonpolar peptides.[20] One possible explanation for these results is the lack of an efficient cationization agent on as-prepared PGaN, especially given that the physical attributes of PGaN compare favorably with those of porous Si. However, porous Si possesses a multitude of cation(proton) sources in the form of its(oxide) surface-terminated functional groups; GaN does not. Metal nanoparticles have recently received increasing attention as matrix materials for mass spectrometry. Under UV-irradiation, surface Ag can act as a source of $Ag^+$ available to form adducts with analytes, resulting in cationization. A second factor is that Ag clusters, exhibiting strong LSPR, can extend the intrinsic absorption of GaN to lower photon energies, thereby aiding efficient energy transfer to proximal analytes. Both of these factors motivate the study of Ag-decorated PGaN as a substrate for LDI-MS.

**Ag-Coated PGaN Membrane Characterization.** Different approaches to the formation of porous membranes would be expected to give rise to distinct porous morphologies. As shown in Figure 1, the preparation of porous GaN by Pt-assisted electroless etching under UV-irradiation produces PGaN with nanometer-scale pores with an anisotropic 3D branched structure. PGaN etched for 60 min exhibits a large density of pores (∼$10^9$ $cm^{-2}$) with a ∼500 nm average depth and 80−100 nm average diameter at the orifice. Although other etching techniques, such as the UV-assisted electrochemical method, create more uniform pore diameters,[46] the branched

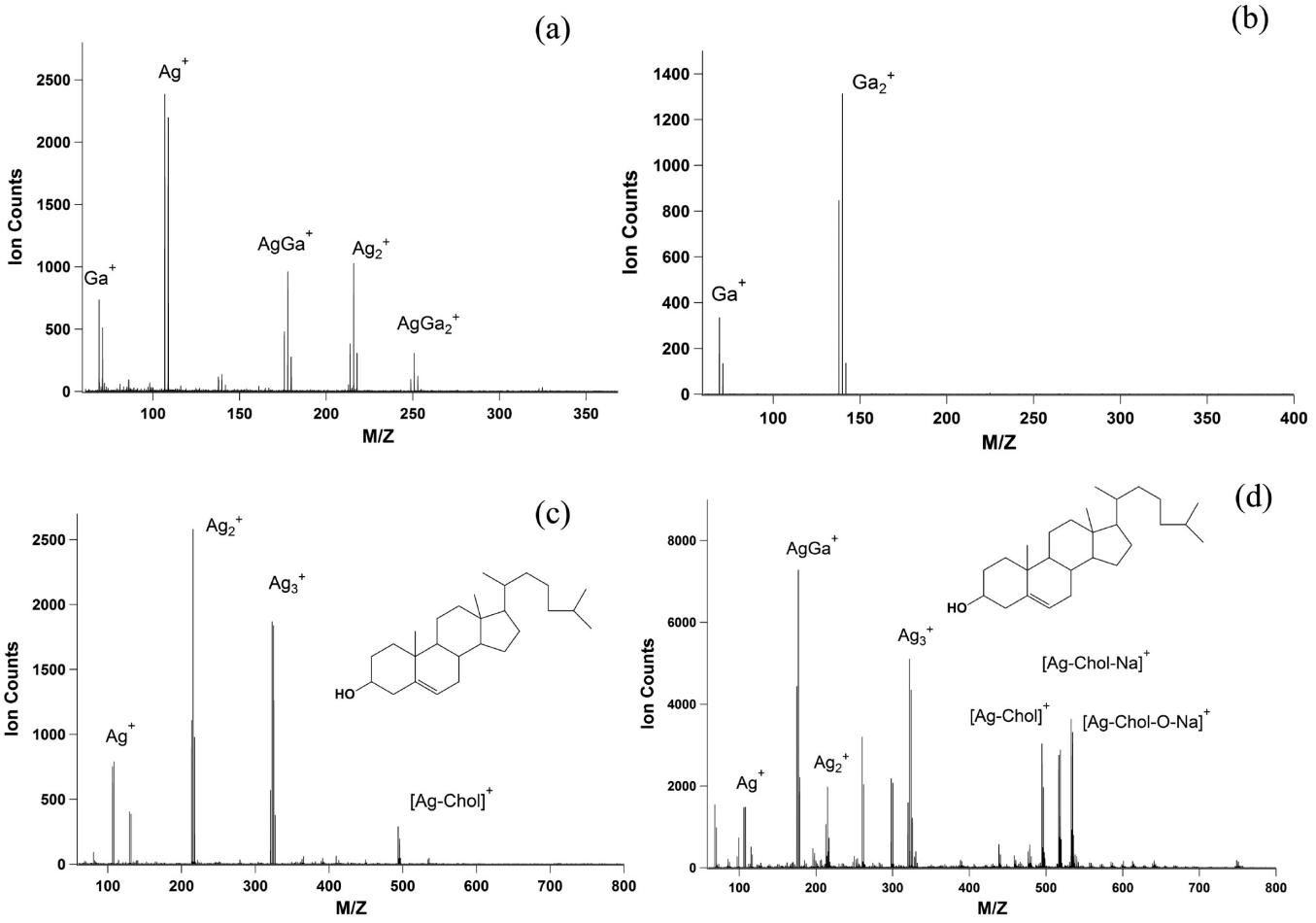


**Figure 3.** LDI time-of-flight mass spectra of 10 picomoles of cholesterol deposited on different substrates: (a) negative control of Ag-coated PGaN film without analyte, (b) negative control of bare PGaN film + cholesterol, (c) 20 nm Ag nanoparticles + cholesterol, (d) Ag-coated PGaN + cholesterol. In each case, the *y*-axis displays the absolute ion count obtained by integration of 200 laser pulses ($t \approx 2$ s).

3D porous structure achieved by the metal-assisted chemical etching process produces a material with a very large surface area available for metal nanoparticle and analyte attachment. Figure 1a shows a plan-view SEM image of Ag-decorated PGaN, and Figure 1b illustrates the cross-section image from the same substrate. The combination of images depicts Ag nanostructures forming on the opening top surfaces and in the interior of the nanopores. Unlike physical adsorption methods which merely deposit Ag particles on the surface and near the mouth of the pores, electroless deposition takes advantage of the extensive internal morphology by depositing Ag both on the top layer and in the pore interiors. After electroless deposition, spheroidal Ag particles are observed throughout the 3D nanopores and attached on interior GaN surfaces indicating that Ag deposition chemistry occurs at a significant depth (~500 nm) below the outer surface, Figure 1b. In addition, the size of PGaN-supported Ag nanoparticles ranges from 20−50 nm depending on reaction time and the $Ag^+$ concentration in the deposition solution, presenting an opportunity to tune the surface morphology, and consequently optimize LDI performance. Finally, Figure 1c shows an energy-dispersive X-ray spectrum which confirms the assignment of the features to a combination of Ag nanoparticles deposited within the anisotropic nanopores produced by the metal-assisted chemical etching process.

Because the substrate must absorb the incident laser radiation in the LDI process, the optical properties of the composite Ag-PGaN material are essential to the quality of the resulting mass spectra. UV−visible extinction spectra in the range 300−800 nm of the materials before and after Ag deposition are shown in Figure 2. As expected, unetched GaN, Figure 2a, is dominated by band-edge absorption(~370 nm) with a weak impurity-related band centered near 650 nm, while metal-assisted chemical etching produces strong band-tail absorption, Figure 2b. The extinction spectrum of Ag nanoparticle-modified PGaN exhibits a strong peak near 420 nm, which is assigned to the LSP resonance of the Ag nanoparticles.[47] The existence of synthesized Ag nanoparticles is also confirmed by energy-dispersive X-ray spectrometry, illustrated in Figure 1c. Because PGaN exhibits band-edge absorption starting at 370 nm, the incident light at wavelengths common to most MALDI-MS instruments(337 nm and 355 nm) is confined to a shallow(~1 $\mu$m) GaN layer. Because this would encompass the entire region containing the GaN nanopores, both the top layer, as well as the Ag-decorated nanopores, can potentially contribute to LDI signal generation.

**LDI Mass Spectrometry from Ag-PGaN.** The primary goal of developing these composite substrates is to realize direct LDI-MS analysis without additional sample preparation. The LDI-MS performance of Ag-PGaN substrates was initially tested in two negative control experiments:(a) no analyte

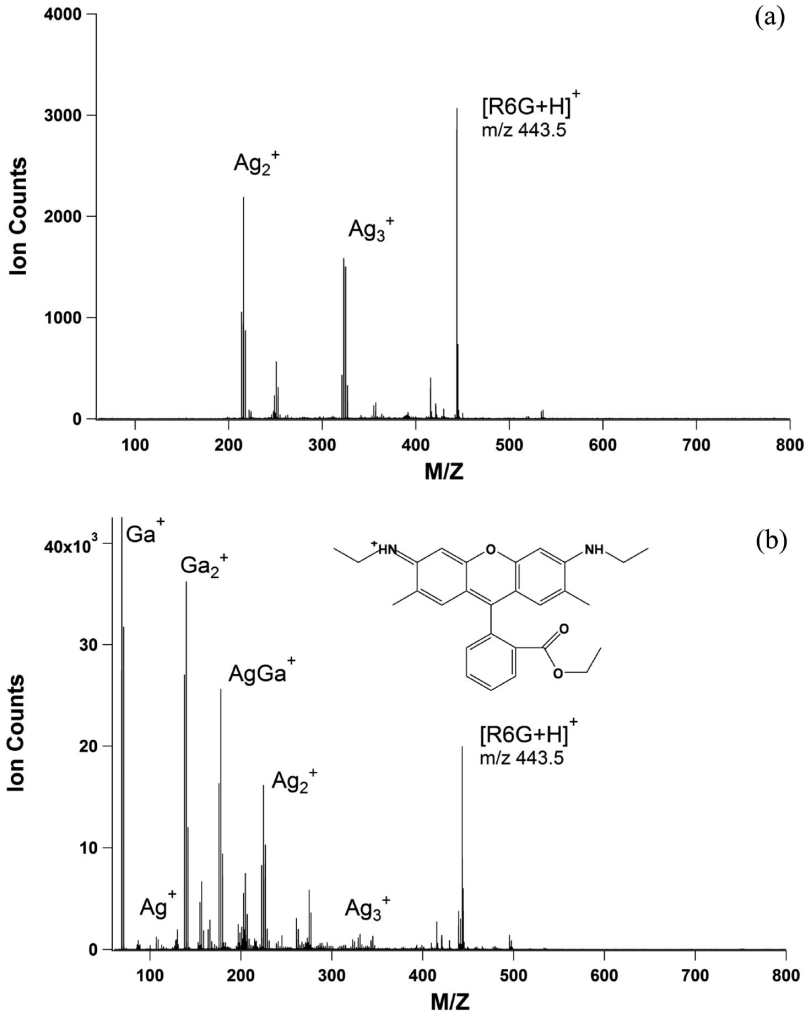


**Figure 4.** LDI time-of-flight mass spectra of 1 picomole of Rhodamine 6G applied to two substrates: (a) 20 nm Ag nanoparticles on unetched GaN; (b) Ag-coated PGaN surface. The *y*-axis displays the absolute ion count obtained by integration of 200 laser pulses ($t \approx 2$ s).

present on Ag-PGaN and (b) analyte(cholesterol) present without Ag. The spectra, Figures 3a and b, show background peaks from $Ag_n^+$, $Ga^+$, $Ga_2^+$, and mixed $Ag_nGa_m^+$ clusters, but, consistent with previous reports,[20] no analyte peaks. The lack of signal from unmodified PGaN indicates that it is difficult to generate adducts effectively by conjugating analyte to $Ga^+$. For comparison to the Ag-PGaN surface, 20 nm spherical Ag nanoparticles were deposited on unetched GaN, namely, Figure S1, Supporting Information, and studied under the same irradiation conditions used in Figures 3a and b. As illustrated in Figure 3c, a relatively weak $[Ag\text{-}Chol]^+$ peak was observed from the unetched Ag nanoparticle surface. Formation of the Ag adduct of cholesterol is signified by the presence of the isotopic doublet at $m/z$ = 493.7/495.7. In contrast, combining electrolessly deposited Ag with PGaN produces stronger MS signals, as indicated in Figure 3(d), where multiple cholesterol adducts are observed with high peak resolution: Ag adducts($m/z$ = 493.7/495.7), sodiated Ag adducts($m/z$ = 516.7/518.7), and an oxidized version of this latter species($m/z$ = 532.7/534.7). Importantly, because the spectra were acquired from samples spotted under identical sampling conditions and with the same mass of analyte, a semiquantitative comparison can be performed, which shows that the ion intensity acquired from Ag-PGaN is ∼10-fold larger than that from substrates containing only Ag particles, while the background from $Ag^+$ oligomers remains comparable (ion count ratio, $Ag^+_{PGaN}/Ag^+_{Ag\ only}$ = 1.87; $Ag_2^+{}_{PGaN}/Ag_2^+{}_{Ag\ only}$ = 0.76; $Ag_3^+{}_{PGaN}/Ag_3^+{}_{Ag\ only}$ = 2.73, see Supporting Information for details). Ion signals are also observed arising from $AgGa^+$($m/z$ 175/177/179) and associated clusters from Ag-coated PGaN, however, these ions occur at a small number of well-defined MS positions and do not significantly interfere with the Ag-analyte adduct peaks of analytical utility. This is consistent with the observation of negligible ion background at masses >300 Da (Figure 3a), which is advantageous for the use of Ag-PGaN in LDI-MS. The enhanced signals obtained from Ag-PGaN relative to Ag nanoparticles alone can be ascribed to a combination of effects. The high density porous structure provides enhanced surface area for both analyte adsorption and anchoring of Ag nanostructures, while the strong optical absorption and thermal properties of GaN aid in the transfer of excitation energy to the analytes for desorption/ionization.

Previous work on Ag-adduct mass spectrometry highlighted the role of C=C double bonds in adduct formation.[48] The Dewar–Chatt–Duncanson model[49,50] proposes two possible bonding mechanisms to explain $Ag^+$–olefin interactions and account for the preferential ionization on Ag surfaces. The free s-orbital in $Ag^+$ can bond with the electron-rich $\pi$-orbital of olefins. Likewise, a $\pi$-bond is obtained by the interaction of the filled d-orbitals of $Ag^+$ and the vacant molecular $\pi^*$-orbitals.

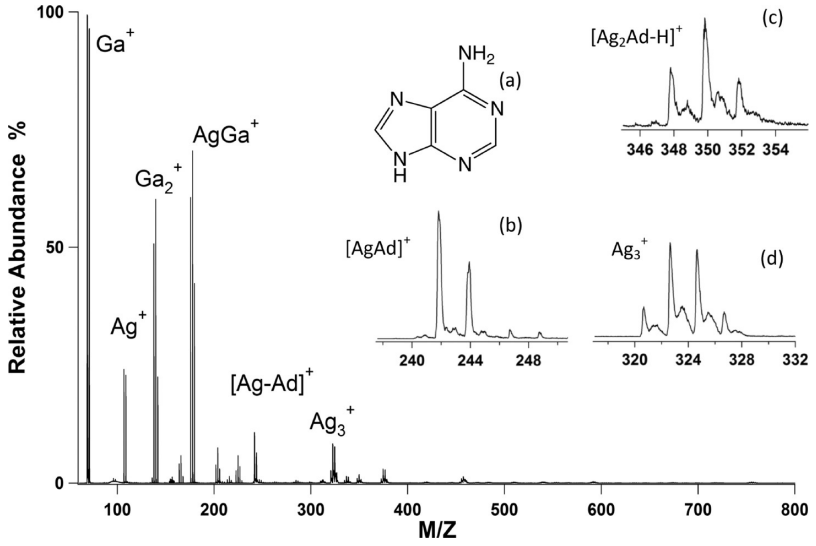


**Figure 5.** LDI time-of-flight mass spectrum of 50 picomoles of adenine deposited on Ag-PGaN. *Inset*: (a) Chemical structure of adenine; (b) $[AgAd]^+$ ($m/z$ 242 and 244); (c) $[Ag2Ad\text{-}H]^+$ ($m/z$ 348/350/352); (d) $Ag3^+$ cluster with ion intensity ratio of 1:3:3:1, in accordance with a simple Poisson distribution of Ag isotopes (107Ag: 109Ag ≈ 51:49).

These bonding models would apply to cholesterol with an olefin unit and pair of electrons available to interact with $Ag^+$. In addition, previous work in this laboratory identified ionization of Ag adducts as an important intermediate in the ionization of thiols and amines on Ag nanoparticle surfaces.[51] In particular, the observation of a mass deficient ion from organomercatans can only be explained by the ionization of a Ag atom adduct which can dissociate to produce either $Ag^+$ or the M-1 mass deficient molecular ion.

Based on these results, the characteristics most likely contributing to the enhanced LDI from Ag-PGaN samples are surface morphology, absorption cross-section, and the efficiency of thermal transfer from lattice to analytes. To help define the roles that these factors play in the ion production process, LDI-MS experiments were conducted on Ag-decorated anodic aluminum oxide(AAO) membranes exhibiting 100 nm pores in an approximate hexagonal close-packed arrangement. Although the same electroless deposition approach was used to coat Ag on the AAO membrane, no detectable signals were observed from spotting 10 picomoles of cholesterol(same conditions used in Figure 3); the resulting mass spectrum (Figure S2, Supporting Information) exhibited only peaks from Ag clusters, mainly dimers. In comparing LDI-MS from Ag-PGaN and Ag-AAO, specific heats(490 J $kg^{-1}$ $K^{-1}$ for GaN and 880 J $kg^{-1}$ $K^{-1}$ for alumina) are within a factor of 2, while the thermal conductivity of GaN(130 W $m^{-1}$ $K^{-1}$) is roughly 5-fold higher than that of alumina(~25 W $m^{-1}$ $K^{-1}$) at ambient condition(300K).[52−55] Both of these factors would favor energy transfer to the analyte in GaN relative to alumina, however it is not reasonable to ascribe all of the dramatic difference in LDI efficiency between the substrates to thermal properties. Rather, the optical absorption, which is strong at 355 nm for GaN, is orders of magnitude weaker for alumina at the same wavelength, given that its bandgap is in the deep UV.[56] Although the Ag nanoparticles can supply some UV absorption, it is clearly not sufficient to compensate for the difference in bandgap absorption between AAO and PGaN. All of these considerations support the interpretation that a combination of pore architecture, strong UV absorption, and advantageous thermal properties interact to make LDI-MS from Ag-PGaN feasible.

To further explore the LDI properties of Ag-decorated PGaN, a similar set of experiments using Rhodamine 6G(R6G) on different surfaces was performed, *viz*. Figure 4. Since R6G is obtained as the hydrochloride, R6G·HCl, LDI-MS yields the protonated form of the free base, $[R6G+H]^+$ at $m/z$ = 443.5, directly without formation of Ag adducts and analyte ion signals are observed from both substrates − Ag NP on planar-(unetched) GaN and Ag-doped PGaN. Unlike cholesterol, which forms Ag-adducts, R6G, a matrix-like organic salt, yields protonated ions almost exclusively. The same ion product($m/z$ = 443.5) was obtained from control experiments conducted by regular matrix-assisted LDI and electrospray mass spectrometry(Figure S3, Supporting Information). The ion signal of $[R6G + H]^+$ is affected by the presence of Ag only through its effect on coupling laser energy, since Ag-adducts of R6G are not observed. The ion intensity obtained from the Ag-PGaN film is ~8-fold more intense than that from the Ag NPs alone, maintaining other parameters constant. It is also of interest to compare the relative intensities of LDI-MS spectra of R6G which scale in the order $I$(PGaN, no Ag) < $I$(Ag NPs) < $I$(Ag-PGaN). Without Ag, it is difficult to observe mass signals of R6G from PGaN, suggesting that even though Ag adducts are not observed, Ag nanostructures still play an important role in the desorption process. This signal enhancement is attributed mostly to the strong UV-absorption of GaN, namely, Figure 2, and the enhanced surface area for AgNP deposition.

To further test this hypothesis and demonstrate the increased ionization efficiency from Ag-PGaN, adenine was employed as a model compound. As addressed previously, Ag nanoparticle based LDI is a selective process and is analyte-dependent.[48] Adenine is less efficiently ionized by Ag nanoparticles, with only Ag cluster ions being observed from 20 nm Ag nanoparticle substrates. However, Ag-PGaN is much more efficient at producing adenine-containing ions, with the principal peak $[AgAd]^+$ at $m/z$ = 242/244 yielding ~$10^4$ ion counts from spotting of 50 picomoles. In addition, a number of more complex cluster ions are observed at higher sensitivity, including a triplet $[Ag_2Ad\text{-}H]^+$ at $m/z$ 348/350/352, and

even a cluster of $[Ag_3Ad\text{-}H]^+$ near $m/z$ 456 attesting to the excellent sensitivity achieved with Ag-PGaN substrates. The observation that the Ag adduct of adenine is easily observed from PGaN, but not from the Ag nanoparticles on a planar surface can be ascribed to a combination of the surface area, optical absorption, and advantageous thermal properties of PGaN, all of which are thought to contribute to signal enhancement for adenine on Ag-PGaN.

**Comparison of Ag-PGaN LDI to Other LDI Approaches.** MALDI has been enormously successful in the study of biomacromolecules deposited on surfaces, so it is important to contrast matrix-free approaches, like the Ag-PGaN LDI method described here, with MALDI and other LDI approaches. Despite its numerous successes, MALDI is not without its challenges, including reproducibility, formation of cocrystallite structures, low spatial resolution and interference in the low molecule weight region(<500 Da).[57,58] These make it difficult to use MALDI quantitatively. The analytical figures of merit for Ag-PGaN LDI may also be compared to those from other forms of LDI, such as Ag nanoparticles in isolation. Under the same MS acquisition conditions, there is a 20-fold signal increase for cholesterol(Figure 3) and ~8× signal increase for R6G (Supporting Information Figure S4) on a Ag-PGaN LDI substrate vs a Ag nanoparticle substrate, yielding a limit of detection of $3 \pm 1 \times 10^{-15}$ mole for R6G. These comparisons point to advantageous application areas for Ag-PGaN LDI, such as the study of catalytic chemistry, where nanoparticulate Ag can serve both as catalyst and matrix. In this context, Ag-PGaN can also facilitate multimodal spectral acquisition on the same sample spot, for example using SERS and LDI-MS.[15]

## CONCLUSIONS

Ag-coated porous GaN substrates made by a two-step protocol of metal-assisted electroless etching to produce PGaN, followed by subsequent electroless Ag deposition supports the LDI-MS of a variety of small molecules, with Ag-adduct formation dominating the mass spectrum for cholesterol and adenine and protonated molecular ions being observed for R6G. Comparisons between Ag nanoparticles on flat substrates and Ag-PGaN highlight the importance of surface area in enhanced ion generation; comparisons of Ag-PGaN to Ag-AAO indicate the role played by the combination of large band-edge absorption of optical radiation and the favorable thermal properties of GaN. The data shown here suggest that Ag-PGaN surfaces serve as an effective LDI medium through a combination of the large surface area, strong optical absorption, and favorable thermal properties of the PGaN coupled with the ability of Ag to produce $Ag^+$ catioization agents. These results further suggest that Ag-PGaN may provide an effective substrate for direct mass analysis over many chemical reactions in restricted space, such as catalytic chemistry and enzymatic processes. Thus, Ag metallization of PGaN presents an attractive candidate for LDI-MS from 3D substrates.

## ASSOCIATED CONTENT

### Supporting Information

Acquisition of SEM images, comparison of signal strength between Ag-PGaN and Ag nanoparticle substrates, and acquisition of R6G MALDI and electrospray mass spectra. This material is available free of charge via the Internet at http://pubs.acs.org.

## AUTHOR INFORMATION

### Corresponding Author

*E-mail: pbohn@nd.edu.

### Present Address

Bei Nie: Chongqing Institute of Green and Intelligent Technology, Chinese Academy of Sciences, Chongqing, People's Republic of China

### Notes

The authors declare no competing financial interest.

## ACKNOWLEDGMENTS

This work was supported by the National Science Foundation IDBR program NSF0852741(materials/instrument support for B.N.), the Department of Energy Office of Biological and Environmental Research DE-SC0006642(support of B.K.D.), and the Army Corp of Engineers W9132T-07-2-0003.

## REFERENCES

(1) Canham, L. T. *Appl. Phys. Lett.* **1990**, *57*, 1046−1048.
(2) Hirschman, K. D.; Tsybeskov, L.; Duttagupta, S. P.; Fauchet, P. M. *Nature* **1996**, *384*, 338−341.
(3) Jiang, J.; Li, S. B.; Jiang, Y. D.; Wu, Z. M.; Xiao, Z. F.; Su, Y. J. *J. Mater. Sci. Mater. Electron.* **2013**, *24*, 463−466.
(4) Li, D. B.; Sun, X. J.; Song, H.; Li, Z. M.; Chen, Y. R.; Jiang, H.; Miao, G. Q. *Adv. Mater.* **2012**, *24*, 845−849.
(5) Liu, L.; Edgar, J. H. *Mater. Sci. Eng. R-Rep.* **2002**, *37*, 61−127.
(6) Soldatenkov, F. Y.; Ulin, V. P.; Yakovenko, A. A.; Fedorova, O. M.; Konnikov, S. G.; Korol'kov, V. I. *Tech. Phys. Lett.* **1999**, *25*, 852−854.
(7) Hedrich, F.; Billat, S.; Lang, W. *Sens. Actuators, A* **2000**, *84*, 315−323.
(8) Seo, J. S.; Whang, D.; Lee, H.; Jun, S. I.; Oh, J.; Jeon, Y. J.; Kim, K. *Nature* **2000**, *404*, 982−6.
(9) Anglin, E. J.; Cheng, L. Y.; Freeman, W. R.; Sailor, M. J. *Adv. Drug Delivery Rev.* **2008**, *60*, 1266−1277.
(10) Aluri, G. S.; Motayed, A.; Davydov, A. V.; Oleshko, V. P.; Bertness, K. A.; Sanford, N. A.; Mulpuri, R. V. *Nanotechnology* **2012**, *23*, 175501.
(11) Duan, B. K.; Bohn, P. W. *Analyst* **2010**, *135*, 902−907.
(12) Li, H. F.; Han, H. M.; Wu, Y. G.; Xiao, S. J. *Appl. Surf. Sci.* **2010**, *256*, 4048−4051.
(13) Lin, V. S. Y.; Motesharei, K.; Dancil, K. P. S.; Sailor, M. J.; Ghadiri, M. R. *Science* **1997**, *278*, 840−843.
(14) Sohn, H.; Letant, S.; Sailor, M. J.; Trogler, W. C. *J. Am. Chem. Soc.* **2000**, *122*, 5399−5400.
(15) Nie, B.; Duan, B. K.; Bohn, P. W. *J. Raman Spectrosc.* **2012**, *43*, 1347−1353.
(16) Paczesny, J.; Kaminska, A.; Adamkiewicz, W.; Winkler, K.; Sozanski, K.; Wadowska, M.; Dziecielewski, I.; Holyst, R. *Chem. Mater.* **2012**, *24*, 3667−3673.
(17) Seol, M. L.; Choi, S. J.; Baek, D. J.; Park, T. J.; Ahn, J. H.; Lee, S. Y.; Choi, Y. K. *Nanotechnology* **2012**, *23*, 095301.
(18) Williamson, T. L.; Guo, X.; Zukoski, A.; Sood, A.; Diaz, D. J.; Bohn, P. W. *J. Phys. Chem. B* **2005**, *109*, 20186−20191.
(19) Cheng, Y. C.; Chen, K. H.; Wang, J. S.; Hsu, W. L.; Chien, C. C.; Chen, W. Y.; Tsao, C. W. *Analyst* **2012**, *137*, 654−661.
(20) Kruse, R. A.; Li, X.; Bohn, P. W.; Sweedler, J. V. *Analyt. Chem.* **2001**, *73*, 3639−3645.
(21) Law, K. P.; Larkin, J. R. *Analyt. Bioanalyt. Chem.* **2011**, *399*, 2597−2622.
(22) Yam, F. K.; Hassan, Z. *Phys. B: Condens. Matter* **2008**, *403*, 3105−3109.
(23) Matoussi, A.; Ben Nasr, F.; Salli, R.; Boufaden, T.; Guermazi, S.; Fitting, H. J.; Eljani, B.; Fakhfakh, Z. *Mater. Lett.* **2008**, *62*, 515−519.
(24) Yam, F. K.; Hassan, Z. *J. Optoelectron. Adv. Mater.* **2008**, *10*, 396−399.

(25) Ryu, S. W.; Zhang, Y.; Leung, B.; Yerino, C.; Han, J. *Semicond. Sci. Technol.* **2012**, *27*, 015014.
(26) Kaminska, A.; Weyher; Waluk, J.; Gawinkowski, S.; Holyst, R. *XXII Int. Conf. Raman Spectrosc.* **2010**, *1267*, 954−955.
(27) Chiu, S. Y.; Huang, H. W.; Liang, K. C.; Huang, T. H.; Liu, K. P.; Tsai, J. H.; Lour, W. S. *Semicond. Sci. Technol.* **2009**, *24*, 045007.
(28) Yam, F. K.; Hassan, Z. *Appl. Surf. Sci.* **2007**, *253*, 9525−9528.
(29) Eickhoff, M.; Ambacher, O.; Steinhoff, G.; Schalwig, J.; Neuberger, R.; Palacios, T.; Monroy, E.; Calle, F.; Muller, G.; Stutzmann, M. *GaN Relat. Alloys—2001* **2002**, *693*, 781−792.
(30) Wang, X. H.; Wang, X. L.; Feng, C.; Yang, C. B.; Wang, B. Z.; Ran, J. X.; Xiao, H. L.; Wang, C. M.; Wang, J. X. *Microelectron. J.* **2008**, *39*, 20−23.
(31) Burlingame, A. L.; Boyd, R. K.; Gaskell, S. J. *Analyt. Chem.* **1998**, *70*, 647R−716R.
(32) Lin, Y. S.; Chen, Y. C. *Anal. Chem.* **2002**, *74*, 5793−5798.
(33) Cha, S.; Yeung, E. S. *Anal. Chem.* **2007**, *79*, 2373−2385.
(34) Zhang, H.; Cha, S.; Yeung, E. S. *Anal. Chem.* **2007**, *79*, 6575−6584.
(35) Lu, M.; Lai, Y.; Chen, G.; Cai, Z. *Anal. Chem.* **2011**, *83*, 3161−3169.
(36) Castro, A. L.; Madeira, P. J. A.; Nunes, M. R.; Costa, F. M.; Florencio, M. H. *Rapid Commun. Mass Spectrom.* **2008**, *22*, 3761−3766.
(37) Gholipour, Y.; Giudicessi, S. L.; Nonami, H.; Erra-Balsells, R. *Anal. Chem.* **2010**, *82*, 5518−5526.
(38) Greving, M. P.; Patti, G. J.; Siuzdak, G. *Anal. Chem.* **2011**, *83*, 2−7.
(39) Northen, T. R.; Yanes, O.; Northen, M. T.; Marrinucci, D.; Uritboonthai, W.; Apon, J.; Golledge, S. L.; Nordstrom, A.; Siuzdak, G. *Nature* **2007**, *449*, 1033−1036.
(40) Akasaki, I. A., H. *Jpn. J. Appl. Phys.* **1997**, *36*, 5393−5408.
(41) Chattopadhyay, S.; Bohn, P. W. *J. Appl. Phys.* **2004**, *96*, 6888−6894.
(42) Chattopadhyay, S.; Li, X. L.; Bohn, P. W. *J. Appl. Phys.* **2002**, *91*, 6134−6140.
(43) Diaz, D. J.; Williamson, T. L.; Adesida, I.; Bohn, P. W.; Molnar, R. J. *J. Appl. Phys.* **2003**, *94*, 7526−7534.
(44) Li, X.; Bohn, P. W. *Appl. Phys. Lett.* **2000**, *77*, 2572−2574.
(45) Diaz, D. J.; Williamson, T. L.; Adesida, I.; Bohn, P. W.; Molnar, R. J. *J. Vac. Sci. Tech. B* **2002**, *20*, 2375−2383.
(46) Vajpeyi, A. P. T., S.; Chua, S. J.; Fitzgerald, E. A. *Phys. E* **2005**, *28*, 141−149.
(47) Prema, P.; Raju, R. *Biotechnol. Bioprocess Eng.* **2009**, *14*, 842−847.
(48) Sherrod, S. D.; Diaz, A. J.; Russell, W. K.; Cremer, P. S.; Russell, D. H. *Anal. Chem.* **2008**, *80*, 6796−6799.
(49) Morris, L. J. *J. Lipid Res.* **1966**, *7*, 717−732.
(50) Mingos, D. M. P. *J. Organomet. Chem.* **2001**, *635*, 1−8.
(51) Nie, B.; Masyuko, R. N.; Bohn, P. W. *Analyst* **2012**, *137*, 1421−1427.
(52) Bougrov, V. L., M. E.; Rumyantsev, , S. L.; Zubrilov, A. *Prop. Adv. Semicond. Mater.* **2001**, 1−30.
(53) Jezowski, A.; Danilchenko, B. A.; Bockowski, M.; Grzegory, I.; Krukowski, S.; Suski, T.; Paszkiewicz, T. *Solid State Commun.* **2003**, *128*, 69−73.
(54) Shackelford, J. F.; Alexander, W. *CRC Materials Science and Engineering Handbook*, 3rd ed.; CRC Press: Boca Raton, FL, 2001; p 424.
(55) Sichel, E. K.; Pankove, J. I. *J. Phys. Chem. Solids* **1977**, *38*, 330−330.
(56) French, R. H.; Mullejans, H.; Jones, D. J. *J. Am. Ceram. Soc.* **1998**, *81*, 2549−2557.
(57) Lu, M.; Lai, Y.; Chen, G.; Cai, Z. *Anal. Chem.* **2011**, *83*, 3161−3169.
(58) Zabet-Moghaddam, M.; Kruger, R.; Heinzle, E.; Tholey, A. *J. Mass Spectrom.* **2004**, *39*, 1494−1505.